On the Dynamics of the Florida Current[1]

William J. Schmitz, Jr.[2]

Nova University
Fort Lauderdale, Florida

ABSTRACT

This paper contains selected results from the first in a series of new efforts directed toward establishing an observational basis for testing hypotheses on the dynamics of the Florida Current. These efforts are based on the application of a recently developed free-instrument method for the collection of density and velocity field data at several sections across the Current. The first group in this series of observations was made during 1964–1965 across two sections off Miami, Florida. The dynamics of a short convergent sector are studied within the frame-work of the one-moving-layer approximation. Efforts were made to sample so that the results obtained would be representative of a mean flow; the consistency of the sampling is supported by a 1% continuity check. A significant restriction in the scope of this investigation is the limited downstream coverage attained.

The observed potential vorticity vs transport streamline distribution is characterized by a relatively flat value in the anticyclonic shear zone and by a steep rise in the cyclonic shear zone. Changes in potential vorticity along transport streamlines are 10% or less and are within experimental error throughout most of the Current. The eddy momentum-flux distribution reported earlier for this section of the Current (G.E.K. data) could be associated with $o(10^{-1})$ to $o(1)$ changes in potential vorticity, even over the short (25 km) particle paths examined. A preliminary examination of the corresponding estimates based on free-instrument data leads to the same type of momentum-flux distribution as that reported earlier, but with reduced cross-stream curvature. The newer estimates agree with past estimates to within relative experimental error except at one point in the Current. It is the earlier data at this one point that led to the above $o(1)$ estimate. The results obtained demonstrate that the Current is *essentially* inertial over the scales investigated. The above remarks apply to the interior of the Current; in zones of 3-to-5-km width at the edges of the Current, the shear is abrupt and the momentum transfer is (strongly) from the mean flow.

One-moving-layer inertial models have been integrated and compared with observation in order to illustrate the sensitivity of the current structure to different specifications of the potential vorticity vs transport streamline distribution and to investigate the response of the Current to downstream changes in width. The results show that the retention of higher-order terms in the potential vorticity distribution leads to a cyclonic zone and that the response to convergence is an acceleration in the downstream current component; the associated mass-field adjustment consists of a rise in the depth and an increase in the cross-stream slope of the depth of the isopycnal layer.

1. Accepted for publication and submitted to press 15 October 1968.

2. Present address: Woods Hole Oceanographic Institution, Woods Hole, Massachusetts 02543.

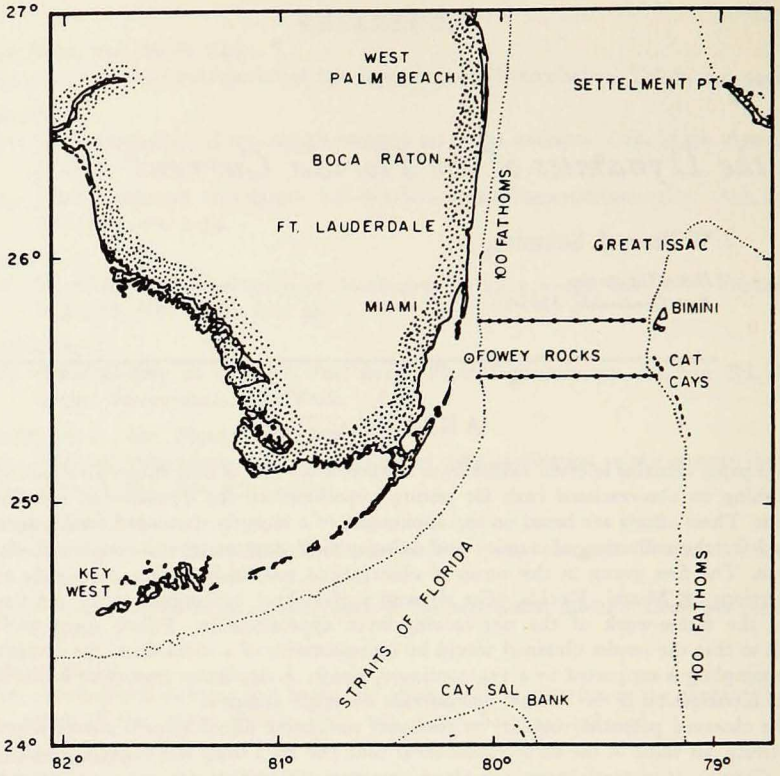

Figure 1. Section and station locations.

Introduction. This paper contains selected results from the first in a series of new efforts directed toward establishing an observational basis for testing hypotheses on the dynamics of the Florida Current. These efforts are based on the application of a recently developed free-instrument method (Richardson and Schmitz 1965) for the collection of density and velocity field data at several sections across the Current. The first group in this series of observations was obtained during 1964–1965 across two sections off Miami, Florida (Fig. 1).

Several previous studies on various features of the current dynamics have been published. Pillsbury's (1890) direct current measurements are an oceanographic classic. Free-instrument results and Pillsbury's results compare favorably (Clausner 1967). Wüst (1924), Parr (1937), and Montgomery (1941) have presented evidence for geostrophic balance of the downstream current component as a first approximation. The first crucial dynamical hypothesis was set forth by Stommel (1953); an order-of-magnitude calculation indicated that the Florida Current might be essentially inertial (at least in the zone of anticyclonic shear). The outline of an experiment that would test this con-

clusion was also presented. Chew (1962) has elaborated somewhat on this idea. Webster (1961, 1962, 1965) studied interactions between the time-averaged current and fluctuations in the surface layer along four sections across the Gulf Stream. In the Florida Current off Miami, he found that these interactions were associated with geostrophic departures of about 10% for the downstream current component.

Stommel (1953) attributed downstream changes in current structure between sections off Key West and Miami to changes in channel width only. Convergence-divergence effects in isolation may be studied locally; this is the procedure that is adopted in this paper. However, the limitation to local downstream coverage is a crucial restriction in scope. The sensitivity of the cross-stream structure to characteristics of the potential vorticity-streamline distribution is also investigated. The study of downstream variations in current structure due to changes in channel width is a necessary prelude to an investigation of larger-scale effects—for example, the investigation of changes in current structure due to changes in Coriolis parameter.

The work by Stommel (1953) was the first that explored the relevance of an inertial-current hypothesis. An analysis of hydrographic data collected near 68°W by Stommel (Deacon *et al.* 1955) suggested that a meaningful local model of the anticyclonic zone in the Gulf Stream could be obtained by specifying a constant potential vorticity across this shear zone. Several theoretical papers on inertial currents have been motivated by these considerations, with initial concentration on homogeneous and two-layer models (Charney 1955, Morgan 1956). Robinson (1965) has formulated a three-dimensional framework for inertial-current models in general, and several specific models based on this theory are being explored. Detailed observational tests on the quantitative range of validity of inertial-current models have not been reported on any scale.

The Data. This section contains a description and discussion of (i) observational method, (ii) pilot data, (iii) sampling considerations, (iv) observational errors, (v) the field program, and (vi) basic observational results.

Observational Method. With reference to Fig. 2, an instrument is launched and falls freely to a preselected depth D (shown as the bottom on Fig. 2); after the weights are released, the instrument returns to the surface under its own buoyancy. The horizontal deflection of the instrument is

$$\vec{X} = \int_{t_0}^{t_1} \vec{V}(x, y, z, t)\, dt; \tag{1}$$

$\vec{V}(x, y, z, t)$ is the horizontal velocity of the instrument (flow) measured in a coordinate system in which x is directed eastward, y northward, and z vertically (positive upward); t is the time coordinate. $\vec{X}$ is measured between points

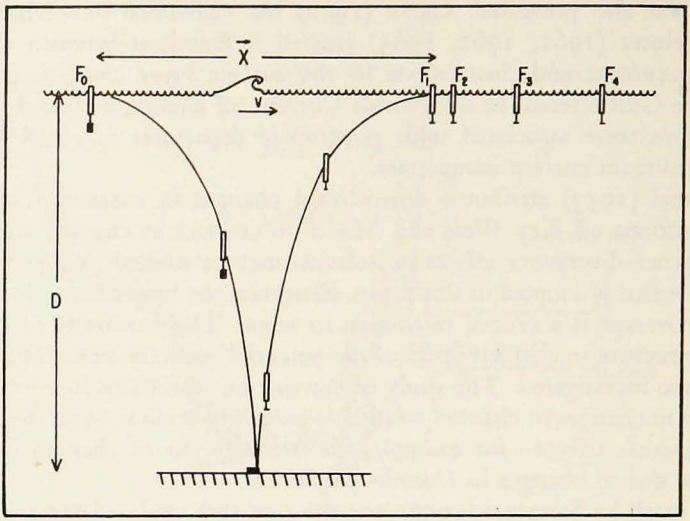

Figure 2. Illustration of the basic elements of the free-instrument method. Each F_i denotes a position-time fix on the free instrument. F_0, F_2, F_3 and F_4 are observed; F_1 is obtained by extrapolation.

F_0 and F_1 at times t_0 and t_1. In treating this Lagrangian measurement as an Eulerian measurement about a mean position, $\vec{V}$ is expanded in a Taylor series in (x, y, t) about a mean coordinate (x_0, y_0, t_0) of the instrument path, and the leading term $\vec{V}(x_0, y_0, z, t_0)$ is retained. The terminal speed of fall (rise), $w = dz/dt = 2D/\tau$, is reached within a few meters after release; τ is the total transit time. Substituting $dt = \tau dz/2D$ in (1) yields

$$\frac{1}{D}\int_{-D}^{0}\vec{V}(x, y, z, t)\,dz \doteq \vec{\vec{V}}(x_0, y_0, D, t_0) = \vec{X}/\tau \qquad (2)$$

for the vertically averaged horizontal velocity to the depth D at the mean coordinate (x_0, y_0, t_0). The attainment of equal fall and rise speeds requires precision ballasting. In practice, somewhat different rise and fall speeds are used. In this case, the leading term is retained in a Taylor-series expansion for $\vec{V}$ over both segments of the instrument path. The results are combined to obtain a formula of the same form as (2); $\vec{\vec{V}}(x_0, y_0, D, t_0)$ is then interpreted to be a weighted average over the two segments of the instrument path.

A combined position-time measurement on the instrument (at the surface) is called a fix (labeled $F_0 - F_4$ in Fig. 2). The F_0 fix is taken as the instrument is dropped; the instrument returns to the surface at F_1; it is then sighted and fixed at F_2 after a short time lapse. The instrument is allowed to drift on the

surface for fixes F_3 and F_4. F_2, F_3, and F_4 are used to determine the surface velocity. F_1 is determined by back extrapolation. Each position-time fix taken in the field is a polaroid photograph of two positioning counters and two digital clocks. The radio navigational system used is known as Hi-Fix (Decca Navigator System, Inc.).

Within the instrument housing, a 16-mm camera takes time-lapse pictures of a pressure gauge, an electric wrist watch, and a mercury thermometer (the sampling interval varied from one to ten seconds).

Each run yields a surface velocity, a vertically averaged velocity to a preselected depth, and a temperature reading at approximately every 20 m of depth. Sigma-t (σ_t) values are calculated directly from temperature measurements by using temperature–σ_t correlations determined from past hydrographic data (Schmitz and Richardson 1966).

Pilot Data. Several preliminary transects across the Florida Current off Miami were completed from August 1964 to April 1965. These transects consisted of from one to several free-instrument drops at 5 to 10 stations. Current-meter records of short duration (a few days), sampled at a relatively high rate (a sample per second), were also obtained. This experience was used to refine techniques, determine error bounds, and investigate sampling criteria. These results have been published in report form (Schmitz and Richardson 1966).

Techniques were developed to the point where a typical crossing of the Current could be completed in a few hours, and the resulting data could be reduced to desired form in a few days. The pilot work indicated that system errors could be held to 10% or less throughout most of the Current. Results from the use of various station spacings indicated that the structure of the Current could be adequately represented by a 10-km station spacing in the anti-cyclonic shear zone and by a 3-to-5-km spacing near the Current edges. The most energetic fluctuations appeared to occur at frequencies in the cycle-per-day range, with characteristic amplitudes of 20 to 30% of the mean for downstream speed and for isopycnal-layer depth and of the same order as the mean for cross-stream speed. In the vertical, smooth distributions were obtained, such that profiles prepared from three or four drops to different depths were not significantly different from those prepared from twice as many drops.

Stommel's (1953) hypothesis of inertial dynamics invoked a two-layer approximation (upper layer moving, lower layer motionless) to actual continuous density and velocity distributions. A method for using this approximation was developed with the pilot data; layers of equal vertically averaged density (σ_t) and vertical averages of horizontal velocity for these layers were extracted from the data and used as observational analogues for the two-layer idealization. It is feasible to schedule a drop to the expected depth of an isopycnal layer and to achieve this goal to within a few tens of meters; the interpolation required to obtain the vertical velocity average to the actual layer depth is

minimized in this fashion. Observations were made at two sections across the Current; these sections were of slightly different width (80 and 86 km) and were separated by 25 km. Within the one-moving-layer approximation, the zone of anticyclonic shear was found to be essentially a zone of constant potential vorticity.

Sampling Considerations. The amount of effort expended in collecting and handling the data and the applicability of the data toward model testing are strongly coupled to sampling criteria; a compromise between practical limitations and potentially rather stringent theoretical requirements is used. Limitations in sampling coverage give rise to crucial restrictions on the scope of the experiment.

In order to test a steady-state theory, it is necessary to obtain stable time averages. In a regime where tidal fluctuations dominate, the samples in time can be approximately randomized in phase over these fluctuations because the periods are well defined. Although the dominant fluctuations are probably of tidal origin, there is a longer period fluctuation present associated with lateral motion of the Current. It seems possible that the correlations reported by Webster (1961) have their origin in this process, ordinary tidal motions being 90° out of phase. About 10 samples over a month were expected to yield reasonably stable averages over fluctuations of this type.

The use of the two-layer idealization in the vertical is motivated by simplicity (a multilevel scheme could be adopted). The particular choice, upper layer $\bar{\sigma}_t = 25.0$, lower layer $\bar{\sigma}_t = 27.0$, is considered in detail. The full set of observations was made across the two sections previously mentioned (Figs. 1, 3). The short downstream separation of these sections is a significant restriction on the scope of the results obtained.

Observational Errors. Three classes of errors are considered: (i) errors associated with the interpretation of a Lagrangian measurement as an Eulerian measurement about a mean coordinate, (ii) system (instrumental and computational) errors, (iii) errors in sampling that result in rectification into time averages. Errors are variable over the area of observation. The present discussion is limited to estimates of characteristic errors; detailed (variable) error estimates may be found in Schmitz and Richardson (1966). The estimates presented are $\pm$, unless otherwise stated.

The justification for neglecting small variations in $\vec{V}$ over drop scales is empirical; in the geographical area of this experiment, instruments dropped at slightly different (x, y, t) yield similar results (within 1 to 3%). Furthermore, some averaging over the space and time scales of a drop is desirable for observations that are to be representative of much larger scales, as is the case here.

Relative positioning errors are of the order of meters, and absolute positioning errors are of the order of tens of meters; this leads to deflection errors of 1 to 5% and to positioning errors of less than 1%. Positioning errors are of one sign. Time errors, about 1 to 3 seconds, lead to time-interval errors of 1 to

3%. Extrapolation errors that occur in obtaining the F_1 fix are 1 to 3%. Depth errors are about 1 to 2%. Typical composite system errors in "quasi-synoptic" vertically averaged velocity components are 5 to 10% in the x component and 3 to 5% in the y component. Errors in the x component may degenerate to 20% at the western edge of the southern transect due to near-baseline positioning errors. Thermometers were calibrated and read to 0.1°. Errors associated with the procedure used to measure and calculate the corrected temperature, the σ_t, the $\bar{\sigma}_t$ distributions, and the layer depths were estimated by comparison with synoptic data from standard hydrographic techniques. Typical errors in quasisynoptic layer depths are 5 to 10%—the critical mass-field-error estimate for the purpose of this study. However, layer-depth errors degrade to 25% at Sts. 1 and 14. Interpolation in depth could lead to an additional error of 1 to 2% in layer-average velocity components. Estimates of system errors for time averages are obtained by dividing the error of a single time sample by the square root of the number of measurements in time.

An upper bound on the bias of a number average by a harmonic term of angular frequency ω averaged over N observations at times t_j is (rectification error)

$$\Delta = \left\{\frac{\alpha^2+\beta^2}{2}\right\}^{1/2}; \tag{3}$$

Δ is the resulting percent error in the mean divided by the percentage ratio of the amplitude of the fluctuating constituent to the mean, and

$$\left.\begin{aligned} \alpha &= \frac{1}{N}\sum_{j=1}^{N} \cos \omega t_j, \\ \beta &= \frac{1}{N}\sum_{j=1}^{N} \sin \omega t_j. \end{aligned}\right\} \tag{4}$$

Within the practical limitations of daytime sampling, an effort was made to minimize Δ for tidal terms. Rectification errors in a time average of layer depth or downstream speed due to tidal fluctuations are estimated to be bounded by 3%. [Eq. (3) has been used to calculate Δ for the various tidal frequencies with the observed t_j; estimates of the relative amplitudes were specified; and individual errors were assumed to combine randomly.] Errors in cross-stream speeds due to this source may reach 25%. The bias due to sampling in the presence of fluctuations at frequencies other than tidal is assumed to be negligible.

The Field Program. The measurements and associated calculations were referred to the (x, y, z) coordinate system previously mentioned; the origin was located at the west end of the Collier Building at The Institute of Marine

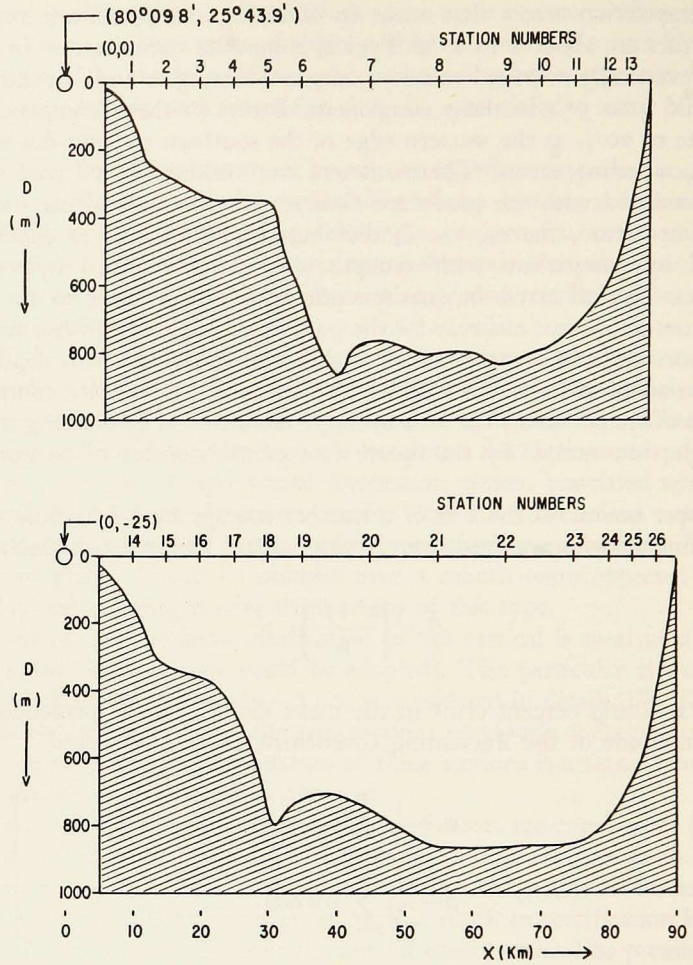

Figure 3. Coordinate system, station positions, and section-depth profiles. The large circle at the left of the upper section denotes the origin of the Cartesian (x, y) coordinate system, located at the specified longitude (west) and latitude (north).

Science, University of Miami, on Virginia Key in Miami, Florida. The geometry of the region under consideration is shown in Fig. 3; the 26 standard station numbers and locations correspond to the dots in Fig. 1. The lateral boundaries of each section, determined by the x position of the 20-m depth curve, are located at $x = 6$ for $y = 0$ and at $x = 5$ and $x = 90$ for $y = -25$ (x and y in kilometers).

Thirteen standard stations were scheduled on each transect. At each station the number of drops and the anticipated depth of each drop were selected by

Table I. Basic data.

1 Stat. no.	2 x coord. (km)	3 Layer depth (m)	4 E/W avg. current comp. (cm/s)	5 N/S avg. current comp. (cm/s)	6 Transp. stream function (20×10^6 m^3/s)	7 Pot. vort. (f/100 m)
WBDY	6	20	0†	0†	0.00†	x
1*	10	58	2	86	0.01	x
2	15	77	5	110	0.02	2.15
3	20	100	7	128	0.05	1.70
4	25	121	12	154	0.09	1.17
5	30	147	12	154	0.14	0.67
6	35	173	9	152	0.20	0.52
7	45	208	12	145	0.34	0.39
8	55	246	8	129	0.50	0.31
9	65	273	9	116	0.66	0.29
10	70	282	7	111	0.74	0.28
11	75	288	12	103	0.81	0.27
12	80	295	11	96	0.89	0.28
13*	83	299	10	94	0.93	x
EBDY	86	20	0†	0†	0.96	x
WBDY	5	20	0†	0†	0.00†	x
14*	10	77	10	94	0.01	x
15	15	92	12	119	0.03	1.87
16	20	126	21	139	0.07	1.13
17	25	146	22	145	0.12	0.76
18	30	173	20	146	0.18	0.53
19	35	200	19	139	0.24	0.42
20	45	233	17	130	0.39	0.36
21	55	265	13	118	0.54	0.28
22	65	286	4	96	0.69	0.24
23	75	305	−3	79	0.82	0.23
24	80	304	−10	67	0.87	0.20
25	83	310	−13	59	0.90	0.16
26*	87	318	−19	46	0.94	x
EBDY	90	20	0†	0†	0.95	x

† Indicates assumed value at boundary.
* Indicates a closure station.
x Indicates value not computed.

matching a pilot cross-stream σ_t distribution, the total depth, and the mid-depth release precision. Drops were scheduled for specified layer depths and for the bottom; from 1 to 3 drops were made at each station occupation. One transect was scheduled for each working day.

Twenty-four transects (12 along each section) were made from 24 May to 24 June 1965. Approximately 700 free-instrument runs were completed. The time of crossing averaged 5 to 6 hours. About 95% of the measurements attempted have been reported (Schmitz and Richardson 1966). The 5% loss was due primarily to: station cancellation as a result of marginal weather

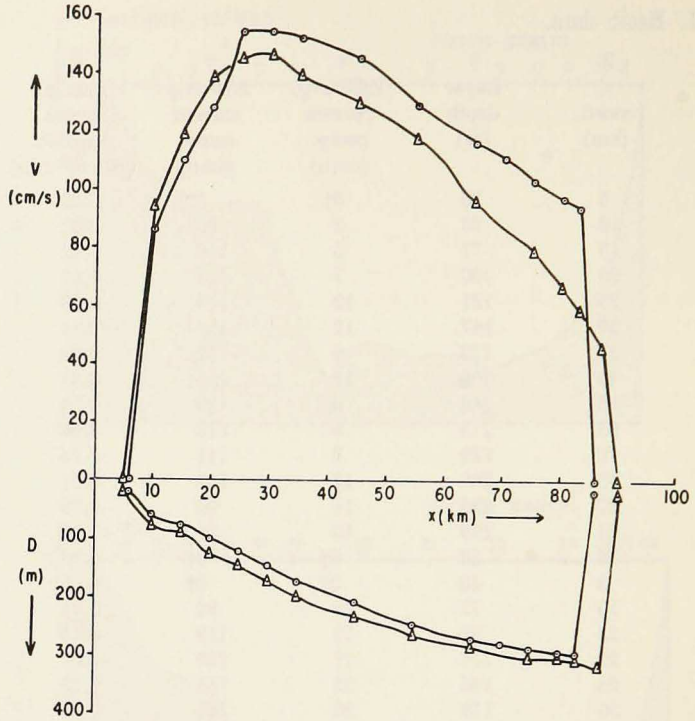

Figure 4. Downstream speed (v) and layer depth (D) vs cross-stream distance (x). Triangles for the southern section and circles for the northern section.

conditions, incomplete or illegible polaroid position fixes, and incomplete or illegible internal film records.

Basic Observational Results. In the following, the symbols (u,v) are used for the (x,y) components of the vertically averaged velocity to the depth D of the layer of equal vertically averaged $\sigma_t, \bar{\sigma}_t = 25.0$; f denotes the Coriolis parameter.

The basic observational results (u, v, and D distributions across the two transects) are listed in Table I and are shown in Figs. 4 and 5. At a station where the total depth is less than the layer depth, the u, v, D data presented are bottom values. These stations are located at the edge of the Current and are called closure stations in order to indicate closure of the layer for a continuity check (marked with an asterisk in Table I). To complete the closure, u and v values (Table I) were brought to zero at the specified Current boundaries.

In the anticyclonic zone, the flow pattern at the southern transect is wider, deeper, and slower than that at the narrower northern transect. However, the Current is decelerating slightly in the cyclonic zone. There are abrupt shear

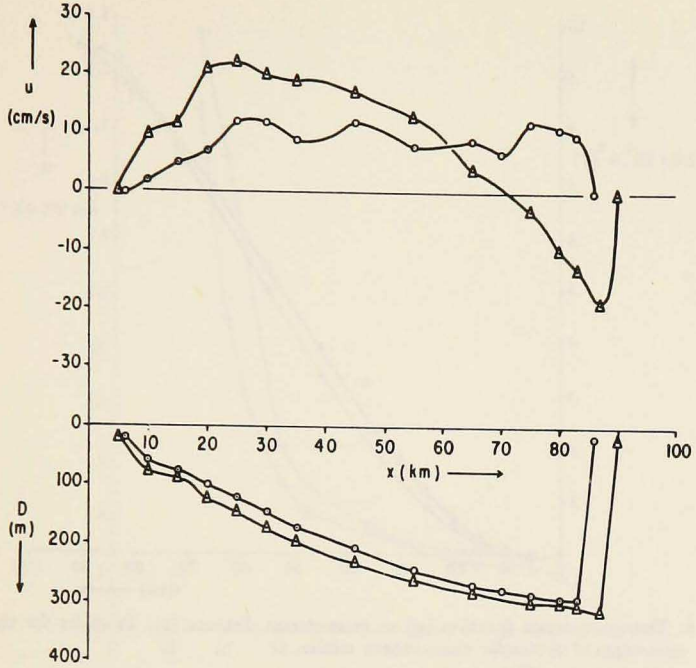

Figure 5. Cross-stream speed (u) and layer depth (D) vs cross-stream distance (x). Triangles for the southern section and circles for the northern section.

zones at the extreme edges of the Current (3 to 5 km in width). Downstream changes in v and D, which vary from station to station but are in the 10 to 20% range, are consistent. The positive values of u on the eastern side of the northern section are possibly due to the location of the northern section at the upstream edge of a divergent sector as well as at the downstream edge of a convergent sector.

Characteristic horizontal shear values in the anticyclonic zone are $-0.2f$—approximately one-half of the typical instantaneous surface values reported for this area on the basis of either free-instrument or GEK observations (Murray 1952). The characteristic horizontal shear in the cyclonic zone is $0.6f$. Instantaneous values of horizontal shear at the surface may be an order of magnitude higher than the time-averaged layer values in the cyclonic zone.

The transport stream function,

$$\psi = \int_{x_0}^{x} v D dx, \tag{5}$$

($\psi = 0$ at $x = x_0$), evaluated for each station and for the boundary points, is listed in Table I, col. 6. Fig. 6 is a plot of $\psi(x)$.

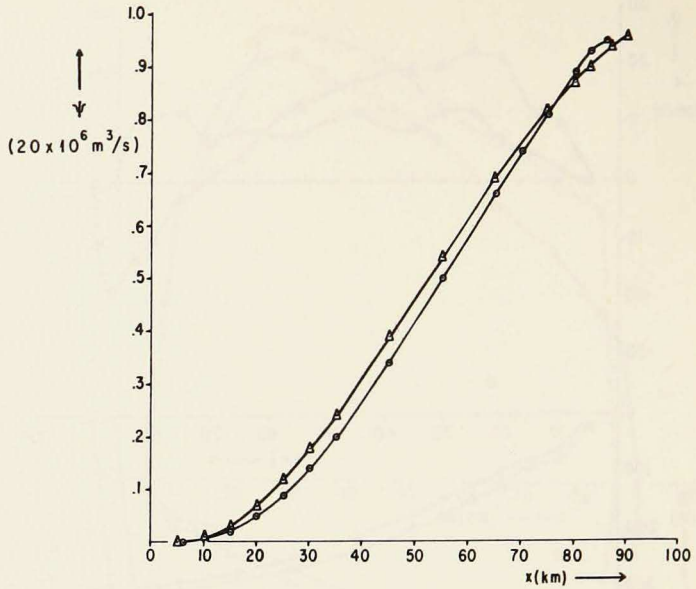

Figure 6. Transport-stream function (ψ) vs cross-stream distance (x). Triangles for the southern section and circles for the northern section.

Compare the total transport of the layer through the two sections. The values of ψ (in units 20×10^6 m^3/s) at the eastern boundary of the Current are 0.96 and 0.95 for the southern and northern sections, respectively—a 1% continuity check. The result of this continuity test is an endoresement of the consistency in sampling.

Discussion. The Potential Vorticity Distribution. Potential vorticity (P) values for interior stations, estimated from

$$P = \frac{v_x + f}{D}, \tag{6}$$

are presented in Table I, col. 7. Coordinate subscripts denote partial differentiation. P values were not calculated for closure stations (marked with an asterisk in Table I) or for boundary points, because D values are not proper layer-depth values at these stations. v_x is a good approximation for the shear contribution to the relative vorticity, even though the y direction is not strictly the downstream direction, in the sense that a chord is a good approximation for the arc of a circular segment of large radius. The curvature term may be estimated for a section midway between the two sections along which observations were made; this effect has been neglected in (6) and is discussed below. Composite

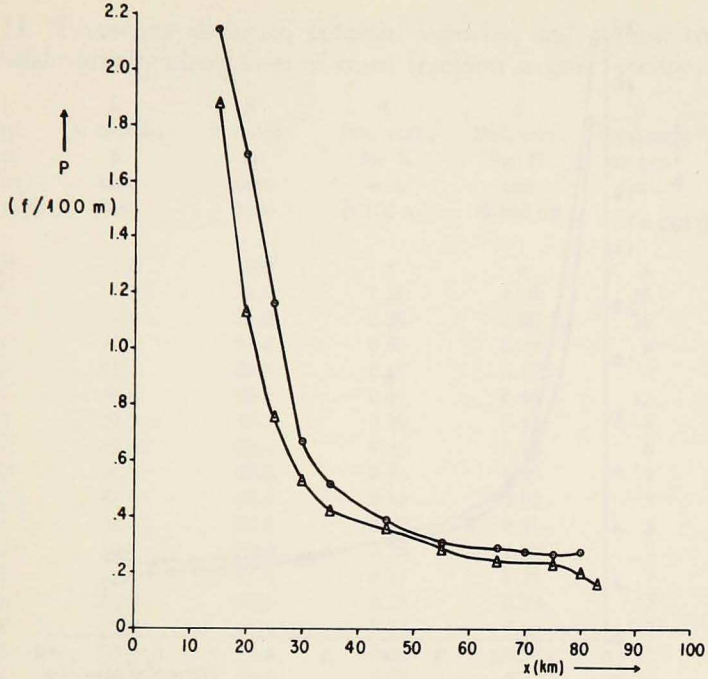

Figure 7. Potential vorticity (P) vs cross-stream distance (x). Triangles for the southern section and circles for the northern section.

errors in the estimates of P by (6), due to observational errors in time-averaged layer depths, downstream speeds, and cross-stream positions, are 5% to 10%.

P is plotted vs x on Fig. 7. Fig. 8 gives the $P(\psi)$ distributions. Potential-vorticity distributions for the two transects coalesce noticeably in ψ relative to x, although deviations of streamlines from lines of constant x are not large (a few kilometers). The basic shape of the $P(\psi)$ distribution is a relatively flat value in the anticyclonic zone, with a steep rise in the cyclonic zone. Changes in P along ψ lines are listed in Table II. Changes in P along ψ lines are essentially within experimental error throughout the bulk of the Current. The changes are consistent; P becomes everywhere more cyclonic (positive).

The approximation of relative vorticity by the shear term leads to errors in P bounded by a few percent, except near the eastern edge of the Current. Curvature effects influence the calculation of percent changes in P along ψ lines only if these effects are different for the two transects. The awkward geometry on the eastern side of the channel at the northern transect is associated with significant streamline curvature near the boundary (as well as mixed convergence-divergence effects). Note in Table II, col. 6 the somewhat large ΔP for the easternmost 20 km of the Current. Estimates of the influence of

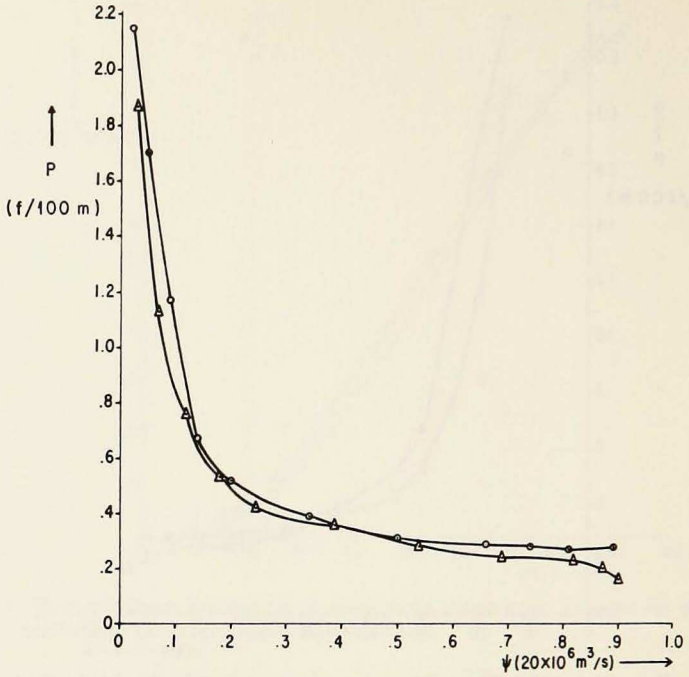

Figure 8. Potential vorticity (P) vs transport-stream function (ψ). Triangles for the southern section and circles for the northern section.

this effect on ΔP values have been made for $\psi \geq 0.55$ at the northern transect (Table II, col. 7). The correction significantly reduces ΔP in this region of the Current.

The demonstration that changes in P along ψ lines are typically 10% or less throughout the bulk of the Current is the crucial evidence that the Current is essentially inertial for the segment of the channel considered. Intuitively, it might be expected that changes in P along particle paths of length only $^1/_3$ of a current width would be small or even insignificant. Pilot data indicated, but did not demonstrate, that this would be the case for at least the anticyclonic zone. If divergent eddy-momentum fluxes had been anticipated to be the crucial element in the local current dynamics, then another type of experiment would have been more appropriate. However, intuitive expectation and inferences from pilot data cannot substitute for the observational demonstration presented. In fact, another set of observations did not rule out the possibility of a much larger ΔP. The influence of interaction between the time-dependent and mean motions enters into the vorticity equation as the integral over a particle path of the second derivatives of the eddy-momentum fluxes. Estimates based on Webster's (1961) results off Miami yield, over particle paths of length

Table II. Transverse positions, potential vorticity, and percent changes in potential vorticity along lines of equal transport stream function.

1 Transp. stream function (20×10 m/s)	2 x coord., S. sect. (km)	3 x coord., N. sect. (km)	4 Pot. vort., for S. sect. (f/100 m)	5 Pot. vort., for N. sect. (f/100 m)	6 % change in pot. vort.	7 % change in pot. vort. with curv. correc.
0.00†	5.0	6.0	x	x	x	x
0.05	17.5	20.0	1.35	1.70	26	26
0.10	23.0	26.0	0.86	1.08	26	26
0.15	27.5	31.0	0.61	0.63	3	3
0.20	32.0	35.0	0.49	0.52	6	6
0.25	36.0	39.0	0.41	0.46	12	12
0.30	39.5	42.5	0.38	0.41	8	8
0.35	42.5	46.0	0.36	0.38	6	6
0.40	45.5	49.5	0.35	0.36	3	3
0.45	49.9	52.5	0.32	0.33	3	3
0.50	53.0	55.0	0.30	0.31	3	3
0.55	56.0	58.0	0.28	0.30	7	7
0.60	59.5	61.5	0.27	0.29	7	5
0.65	62.5	64.5	0.25	0.29	17	12
0.70	66.0	67.5	0.24	0.29	21	16
0.75	69.0	70.5	0.24	0.28	17	10
0.80	73.0	74.5	0.23	0.27	17	3
0.85	78.0	77.5	0.21	0.27	28	8
0.90	83.0	81.0	0.16	0.29	81	52
0.95	90.0	86.0	x	x	x	x

† Indicates assumed value at boundary.
x Indicates value not computed.

25 km, possible changes in P of 5 to 50% (predominantly positive), with the largest changes in the cyclonic zone. The above estimates are based on the cross-stream curvature of the horizontal cross-correlations at the surface only; it was assumed that this one contribution dominates, that the layer-averaged contribution is of the same magnitude as that at the surface, and that the curvature is constant along the particle paths considered.

It has been demonstrated that $o(1)$ changes do not occur on the downstream scale considered and that $o(10^{-1})$ changes occur at only a few points across the Current. A preliminary examination of estimates based on free-instrument data leads to the same type of momentum-flux distribution as that reported by Webster but with reduced cross-stream curvature. The newer estimates agree with Webster's to within his stated experimental error except at one point in the Current. It is his data at this point that led to the above $o(1)$ estimate. The above remarks apply to the interior of the Current; in zones of 3-to-5-km width at the edges of the Current, the shear is abrupt and the momentum transfer is (strongly) from the mean flow.

Now consider possible P changes over larger particle paths (downstream scale). Although definitive estimates of these changes require observations over the appropriate scales of interest, the data in hand may be used to draw inferences about longer downstream-scale behavior. Two examples are discussed. (i) If $o(10^{-1})$ changes occur over particle paths of length $1/3$ of a current width, the $o(1)$ changes might occur over a few current widths. $o(10^{-1})$ changes occur at a few points only—near the Current edges—and smaller changes are not significant with respect to observational error. However, the smaller ΔP are somewhat consistent so that $o(10^{-1})$ changes throughout most of the Current, over particle paths of a few current widths, cannot be ruled out. (ii) The original calculation (Stommel 1953) leading to the notion of inertial-current dynamics is repeated in the next paragraph with the use of the new data.

This calculation is presented as evidence for a predominantly inertial [say $o(10^{-1})$] anticyclonic zone on downstream scales of a few current widths (and is indicative of the relative importance of different processes within the inertial framework). Consider changes in the structure of the anticyclonic zone between a section of the Current off Key West and a section off Miami (downstream separation of a few current widths). Pick a typical streamline in the anticyclonic zone for the $\bar{\sigma}_t = 25.0$ layer (upper layer moving, lower layer motionless), and examine the consequences of P conservation between the two transects. Let ζ denote the relative vorticity; all other symbols have been previously defined. Since the relative vorticity is much less than f at Key West,

$$\frac{\zeta_2+f_2}{D_2} = \frac{\zeta_1+f_1}{D_1} = \frac{f_1}{D_1}, \tag{7}$$

where the subscripts $_{1,2}$ refer to the Key West-Havana (upstream) and Miami-Bimini (downstream) sections, respectively. Also,

$$\frac{\Delta\varrho}{\varrho}(D_2 - D_1) = (h_2 - h_1) = \Delta h, \tag{8}$$

where Δh is the difference in free surface elevation between the sections. A Δh of -4.9 cm along the coast has been observed by leveling between Key West and Miami. The program is to solve for Δh, using (7) and (8), and to compare the results of the calculation with the observed Δh. Thus

$$\Delta h = \frac{\Delta\varrho}{\varrho} D_1 \left(\frac{s+n}{1-n}\right), \tag{9}$$

where

$$\left.\begin{aligned} n &= \frac{f_2 - f_1}{f_2}, \\ s &= \frac{\zeta_2}{f_2}. \end{aligned}\right\} \qquad (10)$$

Stommel specified $\Delta\varrho/\varrho = 2\times10^{-3}$, $D_1 = 250$ m, $s = -.4$; he neglected n to obtain $\Delta h = -20$ cm. Now, this $\Delta\varrho/\varrho$ and D_1 are close to the 25-layer values. However, the s used by Stommel was obtained from GEK measurements at the surface (Murray 1952). The free-instrument data yield characteristic $s = -0.2$; $\Delta h = -10$ cm is obtained from (9) with this s and the above $\Delta\varrho/\varrho$, D_1, n. Furthermore, if the realistic $n = 0.11$ is used ($n \sim s$, not $n \ll s$), then (9) yields $\Delta h = -5$ cm, which is in excellent agreement with observation.

Comparison of Model Results with Observation. Two features of the current dynamics will be explored by comparing the results of simple inertial models with observation: (i) the sensitivity of the cross-stream current structure to specification of the $P(\psi)$ distribution, and (ii) downstream changes in structure due to channel convergence.

The Appendix contains a description of the formulation and integration of governing equations for a uniformly rotating one-moving-layer inertial current in a cylindrical sector of a channel, for three functional approximations to the potential vorticity vs transport-streamline distribution. In the Appendix, and hereafter, the horizontal cylindrical coordinates of the sector (Fig. 9) are denoted by (φ, R); (U,V) are the corresponding velocity components, and H is the layer depth. The central line of the cylindrical sector is oriented in the direction of the Current, and the results obtained apply to either a convergent or divergent sector through the use of a parity ($S = \pm 1$) in the R-component variables. The Appendix also contains formulas for transformation between variables defined in the cylindrical coordinate system and for those defined in the (x, y, z) system on which the observations were based, in particular for $(U, V, H) \rightarrow (u, v, D)$.

The relationship of the model formulation to the actual physical situation is approximate. Averages of products are replaced by products of averages in the advective terms of the momentum equations. Effects due to lower-layer motion and nonuniform rotation are not considered. Nonuniformly convergent geometry is replaced by uniform convergent geometry (the cylindrical sector), and streamline curvature is neglected. In general, the neglected effects are $o(10^{-1})$ with respect to those retained, but not uniformly over the total current sector considered. A detailed discussion of these approximations may be found elsewhere (Schmitz 1966). Cases where neglected effects are of observable influence are discussed as they arise.

Integration of the governing equations requires the specification of up-

stream or inlet conditions. Determination of the upstream conditions by observation and then calculation of the downstream state from the model are anticipated. For the simple case under investigation, it is necessary to specify only the total volume transport and the $P(\psi)$ distribution for the layer at the upstream section. A numerical integration would be required if the full complexity of the observed $P(\psi)$ distribution were to be used.

The procedure followed deviates from the above prescription in two ways. First, the model is integrated analytically for three successively more-realistic functional approximations to the observed $P(\psi)$ distribution. Second, solutions are evaluated for both sections. The motivation for constructing the models is to gain insight into the Current dynamics as opposed to conducting a precision comparison with observation. By considering in turn the solutions from the successive approximations to $P(\psi)$, it is possible to examine the sensitivity of the current structure to the specification of $P(\psi)$. Some redundancy is introduced by evaluating and discussing solutions for the upstream section, due to the cycle: evaluation of $P(\psi)$ from observed fields, fitting of functional forms, and computation of observed fields. The motivation for this step is pragmatic; the introduction of $P(\psi)$ and transport conditions as if determined at another hypothetical upstream transect allows comparison with twice as many observation points as would be the case otherwise. The scheme adopted is in no way used to force answers to questions of direct interest in this paper. The approximate functional forms of the $P(\psi)$ distribution are fitted generally over all of the $P(\psi)$ data.

A detailed comparison of the model with observation requires specification of a set of numerical parameters. There is some arbitrariness in this choice of parameters. The solutions given in the Appendix [(A 17) → (A 19) and (A 28) → (A30)] have been evaluated and are presented in Tables IV and V, respectively, for the particular choice of parameters presented in Table III. These equations are evaluated at the (φ_i, R_i) coordinates corresponding to the observation points (x_i, y_i). Tables I, IV, and V are so organized that the deviations of the model from observation may be selected by a one-to-one comparison of the corresponding columns in these tables. Results have also been obtained by using other parameter sets. These additional results are not presented in detail but are discussed briefly in the last paragraphs of this section. There are certain general characteristics of the models that do not depend critically on a particular choice of parameters, and their relationship to observation will be discussed first.

Table III. Parameters used in evaluating solutions.

$x_0 = 6$ km	$\frac{\Delta\varrho}{\varrho} = 2\times10^{-3}$
$W_0 = 80$ km	$f = 6.33\times10^{-5}$/s
$W_1 = 85$ km	$c = 0.30\times$(f/100 m)
$\Delta y = -25$ km	$A = 0.35$ (f/100 m) $(20\times10^6$ m^3/s$)^{1/2}$
$T = 0.96\times(20\times10^6$ m^3/s)	$B = -0.18$

Table IV. Numerical results for the constant potential vorticity model.

1 Sta. no.	2 x coord.	3 Layer depth (m)	4 Angular current comp. (cm/s)	5 Radial current comp. (cm/s)	6 E/W current comp. (cm/s)	7 N/S current comp. (cm/s)	8 Transp. stream func. (20×10^6 m^3/s)	9 Pot. vort. (f/100 m)
WBDY	6	0	0	270	27	268	0.00	0.30
1	10	33	2	246	24	244	0.01	0.30
2	15	70	4	219	21	218	0.04	0.30
3	20	104	5	196	18	195	0.08	0.30
4	25	133	6	175	15	175	0.14	0.30
5	30	160	6	158	13	157	0.20	0.30
6	35	184	7	143	10	142	0.26	0.30
7	45	226	6	118	6	118	0.40	0.30
8	55	262	5	102	3	102	0.53	0.30
9	65	293	4	91	−1	91	0.66	0.30
10	70	307	3	88	−3	88	0.73	0.30
11	75	321	2	86	−4	86	0.80	0.30
12	80	335	1	85	−6	85	0.87	0.30
13	83	344	0	86	−7	85	0.91	0.30
EBDY	86	352	0	87	−9	86	0.96	0.30
WBDY	5	0	0	266	27	265	0.00	0.30
14	10	52	3	228	23	227	0.02	0.30
15	15	87	4	203	20	202	0.06	0.30
16	20	117	6	181	17	181	0.11	0.30
17	25	145	6	162	14	162	0.16	0.30
18	30	170	7	146	12	145	0.22	0.30
19	35	192	7	131	10	131	0.29	0.30
20	45	230	6	108	7	108	0.41	0.30
21	55	263	5	92	3	92	0.53	0.30
22	65	290	4	81	0	81	0.65	0.30
23	75	316	2	75	−3	75	0.77	0.30
24	80	328	1	74	−4	74	0.83	0.30
25	83	335	1	74	−5	74	0.87	0.30
26	87	345	0	74	−7	74	0.92	0.30
EBDY	90	352	0	75	−8	75	0.96	0.30

The essential information on the sensitivity of the cross-stream current structure in the model to specification of $P(\psi)$ is obtained by comparing the general character of the solutions for the successive analytical approximations to observed $P(\psi)$. The anticyclonic shear zone is a region of constant potential vorticity. The solutions proceed through exponential and then polynomial to trigonometric form as higher-order terms in these approximations are retained. The role of retaining higher-order terms in successive approximations to observed $P(\psi)$ (as demonstrated by this change in the character of the solutions) is basically to bend the V profile down on the western side of the current, leading to the formation of a cyclonic zone there.

Table V. Numerical results for the variable potential vorticity model.

1 Sta. no.	2 x coord. (km)	3 Layer depth (m)	4 Angular current comp. (cm/s)	5 Radial current comp. (cm/s)	6 E/W current comp. (cm/s)	7 N/S current comp. (cm/s)	8 Transp. stream funct. (20×10^6 m^3/s)	9 Pot. vort. (f/100 m)
WBDY	6	0	0	123	13	122	0.00	x
1	10	16	0	129	12	129	0.00	7.57
2	15	38	0	136	11	136	0.01	3.17
3	20	60	0	142	10	141	0.03	1.92
4	25	83	1	146	8	146	0.05	1.34
5	30	107	1	149	7	149	0.09	1.00
6	35	131	1	150	6	150	0.13	0.78
7	45	180	2	149	3	149	0.25	0.52
8	55	227	3	143	0	143	0.40	0.38
9	65	271	3	131	−3	131	0.57	0.29
10	70	292	3	124	−4	123	0.66	0.25
11	75	311	2	115	−6	115	0.75	0.23
12	80	329	2	105	−7	105	0.84	0.21
13	83	339	1	98	−8	98	0.89	0.20
EBDY	86	352	0	88	−9	88	0.96	0.18
WBDY	5	0	0	115	12	114	0.00	x
14	10	25	0	125	11	124	0.00	4.78
15	15	46	0	131	10	131	0.02	2.56
16	20	68	0	136	9	136	0.04	1.69
17	25	90	1	140	8	140	0.07	1.22
18	30	113	1	143	7	142	0.10	0.94
19	35	136	2	144	6	144	0.14	0.75
20	45	182	3	142	3	142	0.26	0.51
21	55	227	3	136	1	136	0.40	0.38
22	65	269	3	124	−2	124	0.56	0.29
23	75	307	3	108	−4	108	0.73	0.23
24	80	324	2	99	−6	99	0.81	0.21
25	83	333	2	92	−6	92	0.86	0.20
26	87	344	1	84	−7	83	0.92	0.19
EBDY	90	352	0	77	−8	76	0.96	0.18

x Indicates value not computed.

The essential information on the downstream variability in the models is contained in the H distribution. H_R is always ≥ 0; H always decreases (rises) and V always increases along lines of equal φ going downstream, except at the very edges of the Current. These increases in V and decreases in H are not uniform, even in a uniformly convergent channel, because of the rotational constraint. The U field shifts mass to the east in order to bring about the adjustment (geostrophic) of the mass field to the acceleration of the downstream-current component in the convergent sector. These two features are basic ingredients of the observed fields; the rise in layer depths is a more

clearly isolatable feature of the data than the increase in the cross-stream slope of D.

In the following discussion of error, the corresponding columns in Tables III and IV are compared with those in Table I. All errors presented are in percent deviation from the appropriate observed value. In the transformation of (U,V) to (u,v), small percentage errors in V may introduce large percentage errors in u on the sides of the Current, especially on the western side. Characteristically, the u-field agreement with observation is much better in the center of the channel than at the edges. Note that, in a detailed comparison, the exclusion of a mechanism providing for shear zones at the Current edges will be of potential significance at exterior stations only, since the observed shear zones are separated in width by only about one station.

As expected, the constant P model does not yield a cyclonic zone. Since a constant P model will not yield realistic downstream-speed values in the cyclonic zone, the value of the constant specified is one appropriate to an anticyclonic zone rather than to an average over the whole current. H differences over all nonclosure stations are an average of 4%, with a standard deviation of 6%. To evaluate the v differences for the anticyclonic zone, values for Sts. 5 to 12 and 18 to 25 are used. An average deviation of -9% and a standard deviation of 13% are obtained.

The variable P model yields a cyclonic zone. In the model relative to the data, the v axis is 5 to 10 km toward the center of the channel. For all of the nonclosure stations, the average v deviation is 10% and the standard v deviation is 14%. The H differences are an average deviation of -25% and a standard deviation of 10%. The H differences are predominantly of one sign and become large percentagewise near the western boundary. If the three stations nearest this boundary are deleted from the previous estimates, an average deviation of -9% and a standard deviation of 14% are obtained. The u deviations are about a factor of 2 less than those for the constant P model.

Model results and error estimates have been presented for one particular choice of parameters for one layer. Results obtained with various parameter sets and with other layers yield agreement with observation for v and D between 5 and 40%; that is, the range of agreement varies by approximately a factor of 2 about the results presented above. The case presented was chosen for illustrative purposes. In all cases, the general features of the models previously mentioned are obtained.

A Remark on the Structure of the Cyclonic Zone. During the process of evaluating the constant potential-vorticity model, it was noticed that a local internal Froude number, defined by

$$F = \frac{V}{[g'H]^{1/2}}, \tag{11}$$

Table VI. Numerical results for the "constant" potential vorticity model with a maximum allowable internal Froude number of 1.

1 Sta. no.	2 x coord. (km)	3 Radial current comp. (cm/s)	4 E/W current comp. (cm/s)	5 N/S current comp. (cm/s)	6 Pot. vort. (f/100 m)
WBDY	6	0	0	0	x
1	10	80	9	80	9.22
2	15	117	13	117	2.81
3	20	143	14	142	1.64
4	25	162	14	161	0.93
5	30	158	13	157	0.44
6	35	143	10	142	0.32
7	45	118	6	118	0.30
8	55	102	3	102	0.30
9	65	91	−1	91	0.30
10	70	88	−3	88	0.30
11	75	86	−4	86	0.30
12	80	85	−6	85	0.30
13	83	86	−7	85	0.30
EBDY	86	87	−9	86	0.30
WBDY	5	0	0	0	x
14	10	101	12	100	5.86
15	15	131	14	130	2.08
16	20	151	15	151	1.28
17	25	162	14	162	0.63
18	30	146	12	145	0.32
19	35	131	10	131	0.30
20	45	108	7	108	0.30
21	55	92	3	92	0.30
22	65	81	0	81	0.30
23	75	75	−3	75	0.30
24	80	74	−4	74	0.30
25	83	74	−5	74	0.30
26	87	74	−7	74	0.30
EBDY	90	75	--	75	0.30

x Indicates value not computed.

began to exceed, in the model, the observed threshold value 1 at about the equivalent location of the observed Current axis. As a heuristic test, the constant P model was evaluated with the added restriction $F \leq 1$; V values were set equal to $[g'H]^{1/2}$ at (φ, R) points where the constant P model yielded $F > 1$. The results of this calculation are presented in Table VI. Recomputed P values are shown in order to indicate the imposed deviations from the "constant" potential vorticity. This "model" yields a cyclonic zone. The v agreement is improved over previous models, with an average deviation of 4% and a standard deviation of 13% for *all* nonclosure stations. The u deviations are improved by about a factor of 2. The U and H values are not changed.

The supercritical nature of shoreward regions of inertial models of the Gulf Stream with respect to F has been noted by Stommel (1965: 115–116), who suggested that one might expect internal hydraulic jumps or oblique shock fronts along the inshore edge of the Stream.

The criterion $F \leq 1$ might be visualized as a parametric restriction associated with the two-layer approximation used. Empirically, different layers would be associated with different F. (For one case studied, $F \leq 0.5$ was the best choice.) It may be that kinetic energy is transferred to internal gravity waves by means of a vertical shear mechanism, and that in the steady state the overall influence of this process, within the framework of the two-layer idealization, is to restrict V (kinetic energy) to be less than or equal to the phase speed of an equivalent long gravity wave on the (hypothetical) internal interface. Note that, in the above calculation, H (potential energy) is held constant. The detailed character of this postulated process is not understood, and the above calculation is clearly an indicative exercise as opposed to a proper dynamical treatment. It is suggested that this mechanism might be significant in the dynamics of the cyclonic zone, particularly in the initial stages of its formation. One might visualize the cyclonic zone as a region of constant F for one-moving-layer models.

Acknowledgments. This paper is based on a dissertation completed under the supervision of W. S. Richardson. R. L. Snyder and P. P. Niiler have made important suggestions in the presentation and interpretation. Support for this work was provided by the Office of Naval Research under contracts Nonr 4008(02) with the University of Miami and NR083-213 with Nova University, and by the National Science Foundation under grant number GP-4763 with the University of Miami.

APPENDIX

This Appendix describes the formulation and integration of governing equations for a uniformly rotating two-layer (upper moving, lower motionless) inertial current in a cylindrical sector of a channel, for three functional forms of the potential vorticity vs transport streamline distribution. Model results are obtained in a cylindrical coordinate system and are to be transformed into the Cartesian coordinate system on which the measurements reported in the text were based, for comparative purposes. The steps necessary for this transformation are specified.

The appropriate governing equations in a cylindrical sector are

$$V = \frac{g'}{fR} H_\varphi, \tag{A1}$$

$$\frac{UV_\varphi}{R} + SVV_R + fU = -g'H_R, \tag{A2}$$

$$S(RVH)_R + (UH)_\varphi = 0. \tag{A3}$$

These equations are strictly analogous to Cartesian counterparts: geostrophic balance for the downstream-current component, inertial balance in the downstream component of the equations of motion, and continuity (Charney 1955, Morgan 1956, Robinson 1963). The cylindrical sector (Fig. 9) has horizontal coordinates (φ, R); the respective velocity components are (U,V). The R component of the cylindrical sector is oriented in the north-south direction at the center of the Current (the parity $S = -1$ for convergence and $S = +1$ for divergence). The Current boundaries are the coordinates $\varphi = 0, 2\theta$; θ is the angular half-width of the channel. The (φ, R) subscripts denote partial differentiation with respect to the indicated coordinate, H is the layer depth, f is the Coriolis parameter, g' is reduced gravity—equal to the gravitational acceleration multiplied by the difference in layer densities and divided by the lower-layer density. $U = R\dot{\varphi}$ and $V = S\dot{R}$; the dots denote time differentiation.

A transport stream function, ψ, is introduced:

$$\left.\begin{aligned} \psi_\varphi &= RVH, \\ \psi_R &= SUH. \end{aligned}\right\} \tag{A4}$$

The first integrals, involving potential vorticity (P) and Bernoulli (B) functions,

$$\frac{\frac{V_\varphi}{R} + f}{H} = P(\psi), \tag{A5}$$

$$\frac{V^2}{2} + g'H = B(\psi), \tag{A6}$$

are obtained in the ordinary way; and $\partial B(\psi)/\partial\psi = P(\psi)$. In the case considered here, the scaling leading to (A1), (A2) is different from that in the normal inertial-current case. Downstream changes are scaled by the ratio of the change in width (ΔW) to the width (W) of the current. Eqs. (A1), (A2) are appropriate for small $\Delta W/W$.

The transport stream function is given by ($\psi = 0$ at $\varphi = 0$)

$$\psi = \frac{g'}{2f}[H^2 - H^2(0, R)], \tag{A7}$$

and the condition of constant transport, T_0, leads to

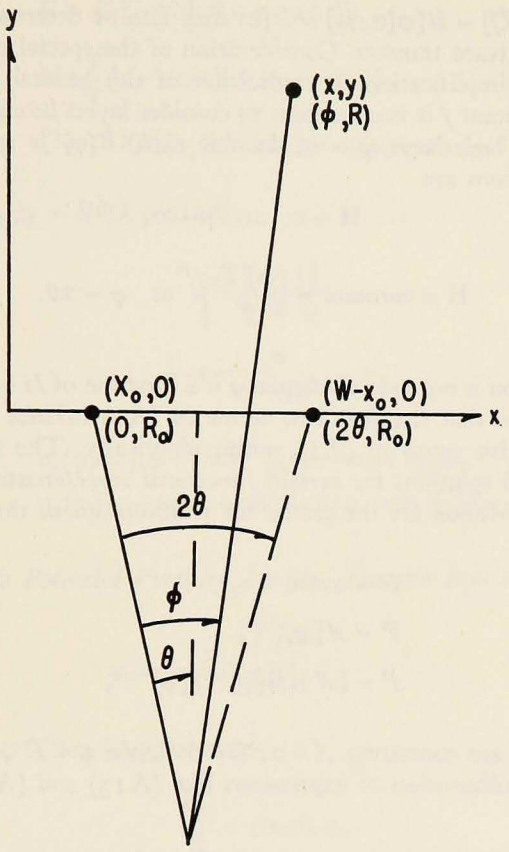

Figure 9. Relationship of the cylindrical (φ, R) and Cartesian (x, y) coordinate systems. R_0 is the value of R at $y = 0$ for $\varphi = 0, 2\theta$ and $x = x_0$, $W - x_0$. W is the width of the Current; θ is the angular half-width of the Current.

$$T_0 = \frac{g'}{2f}[H^2(2\theta, R) - H^2(0, R)]. \tag{A8}$$

The system (A1), (A2), (A3) constitutes three first-order equations, with integration requiring specification of three conditions. Two of these conditions are obtained by specifying $P(\psi)$ and T_0; both are determined at an upstream transect. Since the relationship $\partial B/\partial \psi = P$ and knowledge of P determine B to within a constant only, then a natural third condition is obtained by specifying

$$B(0) = \frac{V^2}{2}(0, R) + g' H(0, R), \tag{A9}$$

where $B[\psi(0,R)] = B[\psi(0,0)] = B(0)$ may also be determined from conditions at the upstream transect. Consideration of the special case of constant f allows a basic simplification in application of the general eqs. (A8), (A9). That is, for constant f it is consistent to consider layers brought to the surface at the western boundary: $\varphi = 0$. In this case, $P(\psi)$ is specified, and the boundary conditions are

$$H = 0 \quad \text{at} \quad \varphi = 0, \tag{A10}$$

$$H = \text{constant} = \left[\frac{2fT_0}{g'}\right]^{1/2} \text{at} \quad \varphi = 2\theta. \tag{A11}$$

The simplification is not only algebraic. ψ is a function of H only. U is geostrophic in the sense that the first two terms in (A2) balance identically. The neglected advective terms in (A1) vanish identically. The possibility of obtaining analytical solutions for certain functional representations of ψ variable P is enhanced. Models are integrated for relationships of the form

$$P = \text{const.} = c, \tag{A12}$$

$$P = A[\psi]^{-1/2}, \tag{A13}$$

$$P = \{A + B[\psi]^{1/2}\}[\psi]^{-1/2}, \tag{A14}$$

where A and B are constants; $A > 0$, $B < 0$. Since $\psi \sim H^2$, the denominator factors for the substitution of expressions like (A13) and (A14) into (A15).

A Constant Potential Vorticity Model. For this case, (A5) becomes

$$\frac{V_\varphi}{R} + f = cH, \tag{A15}$$

where c is a specified constant. With

$$\left.\begin{aligned} \lambda &= \left[\frac{fc}{g'}\right]^{1/2}, \\ \nu &= c\left[\frac{T_0}{2fg'}\right]^{1/2}, \\ \xi &= \frac{R(\varphi - \theta)}{\lambda}, \end{aligned}\right\} \tag{A16}$$

the solutions are

$$V = V_s[\mu \sinh \xi - \varkappa \cosh \xi], \tag{A 17}$$

$$H = \frac{f}{c}[1 - \varkappa \sinh \xi + \mu \cosh \xi], \tag{A 18}$$

$$U = -SV_s[\varepsilon_1(\varphi) \sinh \xi + \varepsilon_2(\varphi) \cosh \xi], \tag{A 19}$$

where $V_s = \lambda f$, $\xi_L = R\theta/\lambda = \xi(2\theta)$,

$$\left.\begin{aligned} \mu &= \frac{(\nu - 1)}{\cosh \xi_L}, \\ \varkappa &= \frac{\nu}{\sin \xi_L}, \end{aligned}\right\} \tag{A 20}$$

and

$$\left.\begin{aligned} \varepsilon_1(\varphi) &= \mu\varphi + \operatorname{csch}^2 \xi_L(\mu + \cosh \xi_L)\theta, \\ \varepsilon_2(\varphi) &= -\varkappa\varphi + \operatorname{sech}^2 \xi_L(\varkappa + \cosh \xi_L)\theta. \end{aligned}\right\} \tag{A 21}$$

Two Variable Potential Vorticity Models. For the first model,

$$P = \left[\frac{A}{\psi}\right]^{1/2}, \tag{A 22}$$

with A constant. Then (A 5) becomes

$$\frac{V_\varphi}{R} = \text{constant}, \tag{A 23}$$

so that this model yields V linear and H parabolic in φ, spreading a linear V profile over both zones of the current. This model is not explored in detail. The next approximation yields the interesting variable potential-vorticity effects.

Consider

$$P = \frac{A + B[\psi]^{1/2}}{[\psi]^{1/2}}, \tag{A 24}$$

with A, B constant, $A > 0$, $B < 0$. The interesting feature is the negative sign of B, so that trigonometric solutions in φ are obtained. Using (A 24), (A 5) becomes

$$\frac{V_\varphi}{R} = A' + BH, \tag{A 25}$$

where

$$A' = -f + A\left(\frac{2f}{g'}\right)^{1/2}. \tag{A 26}$$

With

$$\left.\begin{aligned} \lambda &= \left(\frac{g'}{f|B|}\right)^{1/2}, \\ \nu &= \frac{|B|}{2A'}\left(\frac{2fT}{g'}\right)^{1/2}, \\ \xi &= \frac{R(\varphi-\theta)}{\lambda}, \end{aligned}\right\} \tag{A 27}$$

the solutions are

$$V = V_s[\varkappa \cos \xi - \mu \sin \xi], \tag{A 28}$$

$$H = \frac{A'}{|B|}[1 + \mu \cos \xi + \varkappa \sin \xi], \tag{A 29}$$

$$U = -SV_s[\varepsilon_1(\varphi) \sin \xi + \xi_2(\varphi) \cos \xi], \tag{A 30}$$

where $V_s = \lambda A'$ and $\xi_L = R\theta/\lambda = (2\theta)$,

$$\left.\begin{aligned} \mu &= \frac{(\nu - 1)}{\cos \xi_L}, \\ \varkappa &= \frac{\nu}{\sin \xi_L}, \end{aligned}\right\} \tag{A 31}$$

and

$$\left.\begin{aligned} \varepsilon_1(\varphi) &= -\mu\varphi + (\mu - \varkappa \cot \xi_L)\theta, \\ \varepsilon_2(\varphi) &= \varkappa\varphi + (\mu \tan \xi_L - \varkappa)\theta. \end{aligned}\right\} \tag{A 32}$$

Transformation to the Observational Coordinate System. In the transformation from cylindrical to Cartesian coordinates, layer depth transforms as an absolute scalar. The horizontal coordinates in the two systems are related by

$$\left.\begin{aligned} x &= x_0 + R_0 \sin \theta + R \sin (\varphi - \theta), \\ y &= S[-R_0 \cos \theta + R \cos (\varphi - \theta)]. \end{aligned}\right\} \tag{A 33}$$

R_0 is the value of R at $y = 0$ and $x = x_0$. θ is the angle spanning the half-width of the channel (Fig. 9). Let W_0 be the channel width along $y = 0$ and let W_1 be the channel width at $y = \Delta y$. Δy is the downstream separation of the two sections in a sector. $R_1 = R_0 + \Delta R$ at the edges of the sector where $y = \Delta y$ and $\Delta R \doteq \Delta y$ (to 1%). The widths are chords of circular segments so that

$$\left.\begin{aligned} R_0 &= \frac{SW_0\,\Delta y}{(W_1 - W_0)}, \\ \theta &= \sin^{-1}\frac{S(W_1 - W_0)}{2\,\Delta y}. \end{aligned}\right\} \quad (A\,34)$$

After solutions are obtained in cylindrical coordinates, they are evaluated at the (φ, R) corresponding to observation points in (x, y) coordinates, using the inverse of (A 33):

where

$$\left.\begin{aligned} R &= (x'^2 + y')^{1/2}, \\ \varphi &= \theta + S\tan^{-1}\frac{x'}{y'}, \\ x' &= x - x_0 - R_0\sin\theta, \\ y' &= y + SR_0\cos\theta. \end{aligned}\right\} \quad (A\,35)$$

The corresponding (u, v) are obtained from the (U, V) by

$$\left.\begin{aligned} u &= SV\sin(\varphi - \theta) + U\cos(\varphi - \theta), \\ v &= V\cos(\varphi - \theta) - SU\sin(\varphi - \theta). \end{aligned}\right\} \quad (A\,36)$$

REFERENCES

Charney, J. G.
1955. The Gulf Stream as an inertial boundary layer. Proc. nat. Acad. Sci., *41*: 731–740.

Chew, Frank
1962. The Florida Current as a inertial flow in a uniformly convergent channel. Deep-sea Res., *9*: 131–135.

Clausner, E. J., Jr.
1967. Characteristic features of the Florida Current. Masters Thesis, Univ. of Miami, Coral Gables, Fla. 55 pp.

Deacon, G. E. R., H. U. Sverdrup, Henry Stommel, and C.W. Thornthwaite.
1955. Discussion on the relationships between meteorology and oceanography. J. mar. Res., *14*: 499–515.

Montgomery, R. B.
1941. Transport of the Florida Current off Habana. J. mar. Res., *4*: 198–220.

Morgan, G.W.
1956. On the wind-driven ocean circulation. Tellus, *8*: 301–320.

Murray, K. M.
1952. Short period fluctuations of the Florida Current from geomagnetic electro-kinetograph observations. Bull. mar. Sci. Gulf Carib., *2*: 350–375.

PARR, A. E.
1937. Report on hydrographic observations at a series of anchor stations across the Straits of Florida. Bull. Bingham oceanogr. Coll., *6*: 1–62.

PILLSBURY, J. E.
1890. The Gulf Stream – A description of the methods employed in the investigations, and the results of the research. Rep. U.S. cst. geod. Surv., Append. *10*: 461–620.

RICHARDSON, W. S., and W. J. SCHMITZ, JR.
1965. A technique for the direct measurement of transport with application to the Straits of Florida. J. mar. Res., *23*: 172–185.

ROBINSON, A. R.
1963. Editor's Notes: Wind-driven ocean circulation: a collection of theoretical studies: 153–161. Blaisdell Publishing Company, New York and London. 161 pp.
1965. A three-dimensional model of inertial currents in a variable-density ocean. J. fluid Mech., *21*: 211–223.

SCHMITZ, W. J., JR., and W. S. RICHARDSON
1966. Data Report: A preliminary report on Operation *Strait Jacket*. Inst. Mar. Sci., Univ. Miami, Florida. 222 pp.

STOMMEL, H. M.
1963. Examples of the possible role of inertia and stratification in the dynamics of the Gulf Stream System. J. mar. Res., *12*: 184–195.
1965. The Gulf Stream. 2nd ed. Univ. of California Press, Berkley and Los Angeles; Cambridge Univ. Press, London. 248 pp.

WEBSTER, T. F.
1961. The effect of meanders on the kinetic energy balance of the Gulf Stream. Tellus, *13*: 392–401.
1962. Departures from geostrophy in the Gulf Stream. Deep-sea Res., *9*: 117–119.
1965. Measurements of eddy fluxes of momentum in the surface layer of the Gulf Stream. Tellus, *17*: 239–245.

WÜST, GEORG
1924. Florida- und Antillinström, eine hydrodynamische Untersuchung. Veröff. Inst. Meeresk. Univ. Berl., N.F., (A), Geogr.-naturwiss., *29*: 70 pp. and map.